ASEAN
Journal of Scientific and Technological Reports
Online ISSN:2773-8752

Research article

Nusselt Number Correlation for Elliptical Helical Coils Based on Computational Fluid Dynamics and Experiments

Suriya Sukarin[1], Manusak Janthong[1*], and Sathaporn Thongwik[1]

[1] Faculty of Engineering, Rajamangala University of Technology Thanyaburi, 12120, Thailand
[*] Correspondence: manusak.j@en.rmutt.ac.th

Citation:
Sukarin, S.; Janthong, M.; Thongwik, S. Nusselt number correlation for elliptical helical coils based on computational fluid dynamics and experiments. *ASEAN J. Sci. Tech. Report.* **2026**, *29*(12), e265372. https://doi.org/10.55164/ajstr.v29i12.265372

Article history:
Received: May 5, 2026
Revised: August 21, 2026
Accepted: September 1, 2026
Available online: November 8, 2026

Publisher's Note:
This article is published and distributed under the terms of the Thaksin University.

Abstract: A helical coil is an important component of wrapped helical-coil heat exchangers around an external tank, which helps reduce direct contact between the working fluid in the coil and the fluid inside the tank. Therefore, it is suitable for applications requiring contamination control. However, the design of this type of coil still has limitations, because the correlations used to predict the Nusselt number (Nu), which is an indicator of heat transfer performance, have mostly been developed for circular-cross-section helical coils. Meanwhile, elliptical cross-section tubes have the potential to increase the contact area with the tank wall and modify the flow structure inside the tube. This study investigates the effects of cross-sectional ovality (δ) and coil curvature. (D_h/D_{coil}) , and flow conditions on the Nusselt number (Nu) and internal flow behavior of elliptical helical coils. Three elliptical cross-section coil configurations were used as experimental reference data, and nine computational fluid dynamics simulation cases were conducted under different values of δ and D_h/D_{coil}. The results showed that Nu increased with Reynolds number (Re) and Dean number (Dn), while variations in δ and D_h/D_{coil} modified the secondary-flow distribution and the effectiveness of thermal boundary-layer disturbance. Higher ovality produced a more concentrated asymmetric velocity field, whereas lower ovality resulted in a broader velocity distribution across the tube cross-section. The newly developed correlation predicted Nu with high accuracy, yielding. $R^2 = 0.972$, $MAPE = 5.36\%$, $RMSE = 1.84$, and a cross-validation $MAPE$ of 5.94%, supporting its use within the studied range.

Keywords: Elliptical helical coil; nusselt number; computational fluid dynamics; secondary flow; flow–geometry coupling

1. Introduction

Helical heat exchangers ($HHEs$) are widely used in thermal engineering because of their compact configuration, small installation footprint, and high heat transfer performance compared with straight tubes. This enhanced performance is mainly attributed to tube curvature, which induces secondary flow inside the coil, commonly known as Dean vortices [1, 2]. These vortices promote fluid mixing, thin the thermal boundary layer near the tube wall, and consequently improve convective heat transfer. Owing to these advantages, HHEs have been applied in compact heat exchange systems, waste heat recovery units, and various industrial thermal processes.

Shell-and-helical-coil heat exchangers ($SHHEs$), as illustrated in Figure 1A, are among the most common configurations of HHEs. However, this arrangement

still has limitations in certain applications, particularly because of its complex internal structure, difficulty in cleaning and maintenance, and concerns related to hygiene and contamination control [3, 4]. These issues are especially critical in the food and pharmaceutical industries, where clear fluid separation and ease of maintenance are required. Externally wrapped helical coil heat exchangers ($WHHEs$) have recently been developed as an alternative coil arrangement. In this configuration, the helical coil is installed on the outer surface of the tank rather than being directly immersed in the tank fluid. This design separates the working fluid inside the coil from the fluid inside the tank and reduces the possibility of cross-contamination between the two fluids, as shown in Figure 1B.

In $WHHEs$, the heat transfer path is more complex than that in conventional $SHHEs$. Heat is not transferred directly from one fluid to another; instead, it passes through several layers, including the fluid inside the tube, the tube wall, the coil–tank contact region, and the tank wall before reaching the heat-receiving fluid inside the tank. This coupled heat transfer through both fluid and solid domains is referred to as conjugate heat transfer. Therefore, the design of helical coils for this type of system should not be based only on internal flow behavior inside the tube, but should also account for coil geometry and the contact area between the coil and the tank wall.

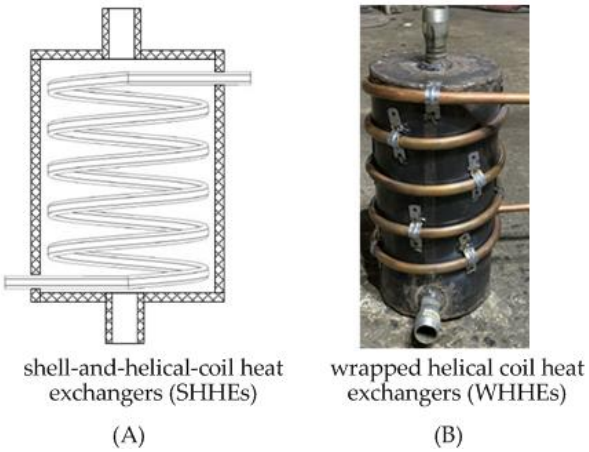


Figure 1. Comparison of (A) shell-and-helical-coil heat exchanger (SHHE) and (B) externally wrapped helical-coil heat exchanger (WHHE) configurations.

Current design knowledge for helical coils in $WHHEs$ applications remains limited. Many studies on $HHEs$ still focus mainly on circular helical coils, particularly in $SHHEs$ systems, where internal flow behavior, Dean-vortex formation, and Nusselt number enhancement are commonly emphasized [5-8]. In contrast, helical coils used in $WHHEs$ configurations require additional consideration of external geometric factors, particularly the coil–tank contact (CTC) region, which is associated with the system-level heat-conduction path. This research gap suggests that Nu prediction correlations developed for circular tube geometries may not accurately describe the heat-transfer behavior of coils with non-circular cross-sections, especially when cross-sectional deformation simultaneously modifies the contact region and the internal flow structure. To address this gap, this study investigates the effects of elliptical helical coil geometry, particularly cross-sectional ovality (δ) and coil curvature, on internal flow behavior and heat-transfer performance. A Nu prediction correlation is then developed to support preliminary design of elliptical helical coils for $WHHE$ applications. This study focuses on flow behavior and heat-transfer characteristics inside elliptical helical coils, with Nu used as the primary performance indicator. A full thermo-hydraulic evaluation of the overall $WHHE$ system is beyond the scope of this work. The study was organized into two connected parts. First, three elliptical coil configurations were experimentally tested to provide real-system reference data for examining heat transfer trends and validating the CFD model. Second, nine CFD cases were arranged as a geometry-based design matrix to systematically extend the analysis of tube cross-sectional shape and coil curvature. This structure allows the combined effects of geometrical variables on heat transfer to be evaluated and supports the development of a Nu prediction model for elliptical helical coils within the investigated parameter range. Compared with previous studies that primarily investigated circular or modified helical tube configurations and

emphasized conventional thermofluid behavior [5-8], the present study focuses specifically on elliptical helical coils and considers the combined effects of cross-sectional ovality and coil curvature. The main contribution of this work is the integration of experimental measurements with a systematic CFD geometry matrix to evaluate the coupled influence of flow and geometry on heat transfer. In addition, a new Nusselt number correlation incorporating Dn, Pr, δ, and D_h/D_{coil} is developed for elliptical helical coils within the investigated parameter range. This approach extends conventional circular-coil correlations by explicitly accounting for the effects of non-circular cross-sectional geometry.

2. Materials and Methods

2.1 Concept and Scope of the WHHE Arrangement in This Study

In this study, the $WHHE$ configuration was used only as a design framework to define the installation arrangement of the helical coil. The work did not aim to evaluate the overall performance of the entire WHHE system. Instead, it focused on the flow behavior and heat transfer characteristics inside elliptical helical coils. Figure 2 presents a conceptual comparison between circular and elliptical tube cross-sections in contact with the tank wall. Compared with a circular tube, an elliptical tube is expected to provide a wider contact region between the tube and the tank wall. Therefore, the quantitative evaluation was based on dimensionless parameters that describe the internal flow and heat transfer behavior of the coil, namely the Re, Dn, Pr, and Nu. These parameters allow coils with different geometrical characteristics to be compared on a common basis.

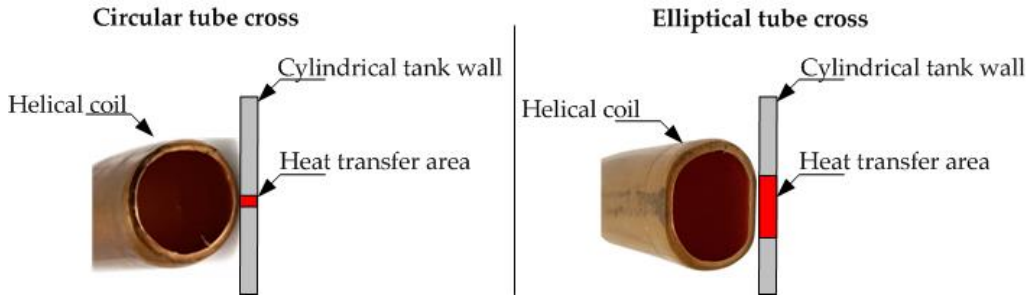
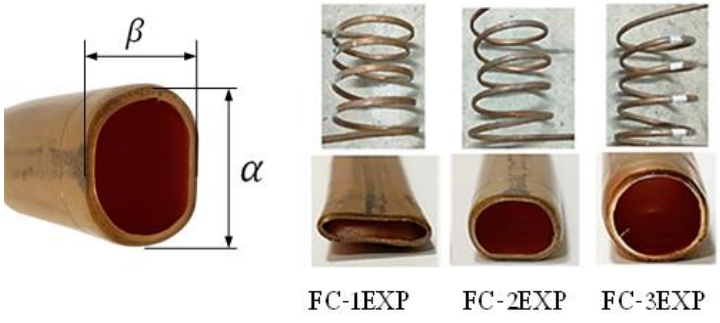


Figure 2. Comparison of heat transfer contact area between circular and elliptical tube cross-sections in externally wrapped helical coil configurations

2.2 Geometrical Design of the Elliptical Helical Coil Samples

The elliptical helical coil samples were designed to provide a database for the experimental investigation and for validating the numerical simulation results. The design focused on the influence of tube cross-sectional geometry on the flow behavior and heat transfer characteristics inside the coil. All experimental samples were fabricated from copper tubes with an initial outer diameter of 10 mm. and a wall thickness of 1 mm. The tubes were then formed into helical coils and reshaped to obtain different levels of δ, as shown in Figure 3.



(A) (B)

Figure 3. Helical coil configurations and tube cross-sections: (A) geometric definition of ovality (δ) and hydraulic diameter (D_h) based on Eqs. (1) and (2); (B) fabricated experimental samples (FC-1EXP to FC-3EXP) corresponding to the parameters listed in Table 1.

In the experimental sample design, the main parameter used to describe the deformation of the tube cross-section was the ovality ratio (δ). This parameter indicates the degree of difference between the major and minor axes of the elliptical tube cross-section, as defined in Equation (1) [9]. A higher δ value represents a more elongated elliptical cross-section, whereas a lower δ value corresponds to a cross-section closer to a circular shape. In addition, the hydraulic diameter (D_h) was used as the characteristic length for calculating the dimensionless parameters related to flow and heat transfer. It was determined from the flow cross-sectional area and the wetted perimeter of the tube, as expressed in Equation (2).

$$\delta = \frac{(\alpha-\beta)}{\varphi} \times 100 \quad (1)$$

where $\varphi = \frac{\alpha+\beta}{2}$

$$D_h = \frac{4A_c}{P_w} \quad (2)$$

where α and β are the major and minor dimensions of the elliptical tube cross-section, respectively; A_c is the internal cross-sectional flow area; and P_w is the wetted perimeter of the tube cross-section.

2.3 Experimental Setup and Measurement System

The experimental setup was arranged to evaluate the heat transfer behavior of elliptical helical coils under controlled operating conditions. Three experimental coil samples, namely FC-1EXP, FC-2EXP, and FC-3EXP, were tested. These samples had different geometrical characteristics, as summarized in Table 1.

Table 1. Summary of geometric parameters, hydraulic diameter, and heat transfer surface area of the tested helical coil configurations

Sample	δ (%)	$\frac{D_h}{D_{coil}}$	D_h (m)	D_{coil} (m)	Surface area (m^2)	Length (m)
FC-1EXP	66.67	0.062	0.0111	0.18	0.1121	2.2457
FC-2EXP	33.33	0.067	0.012	0.18	0.1093	2.2457
FC-3EXP	50.00	0.065	0.0117	0.18	0.1107	2.2457

The main role of these three experimental cases was to provide real-system reference data for confirming the basic heat transfer trends and for assessing the reliability of the CFD model before extending the analysis to the nine geometrical cases. Therefore, the experimental part of this study was not intended to cover the full geometrical range of elliptical helical coils. Instead, it served as an experimental reference for validating the numerical model. The flow diagram of the experimental system is shown in Figure 4(A).

Water was used as the working fluid in this study because of its suitable thermal properties, safety, high stability, and wide use as a reference fluid in both experimental and numerical studies of helical coil heat exchangers. These characteristics make water appropriate for generating comparative data and validating the CFD model [1, 10]. The inlet water temperature of the coil (T_{in}) was maintained at 50 °C using a hot water tank equipped with a temperature control system, as shown in Figure 4B. The temperature of the water outside the coil was controlled at 30 °C to provide a constant external boundary condition throughout the experiment. The working-fluid flow rate was varied from 0.5 to 2.5 L/min and measured using a flow meter. The measured flow rate was then used to calculate the mass flow rate ($\dot{m}$), which is a key parameter for evaluating the heat transfer rate. Temperature measurements were performed using calibrated K-type thermocouples installed at the coil inlet (T_{in}) and outlet (T_{out}) to determine the temperature change of the working fluid. Additional thermocouples were also installed along the coil at angular positions of 360°, 720°, 1080°, and 1440°, as shown in Figure 4C, to record the temperature variation along the flow path inside the tube. These locations cover the flow development region in the helical coil and provide supporting data for analyzing the heat transfer behavior inside the coil. The thermocouple signals were recorded using a data acquisition system, as shown in Figure 4C. The system had a 16-bit resolution and an accuracy of ±0.1%. The measured signals were transmitted through an RS485 MODBUS RTU system for continuous data recording. The main experimental

uncertainty was associated with the K-type thermocouples, which had an accuracy of ±0.5 °C, together with the uncertainties of the data acquisition system and flow-rate control. The experimental data were used to calculate the heat transfer rate, heat transfer coefficient, and Nusselt number, and were also used as reference data for validating the CFD model.

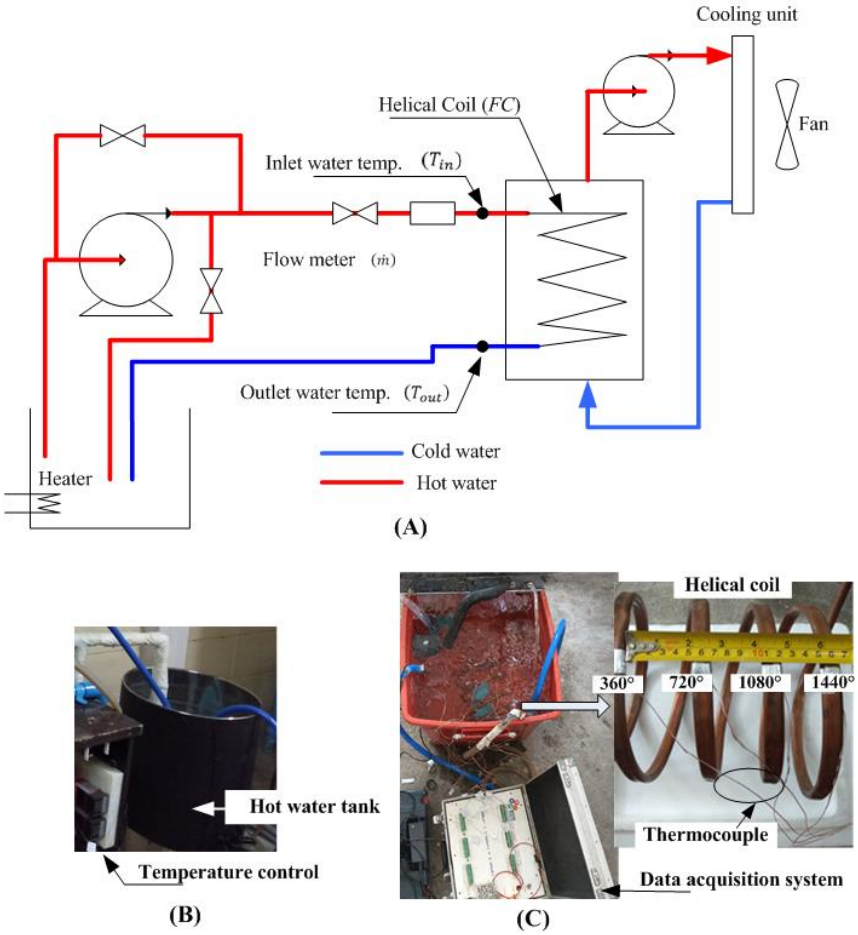


Figure 4. Experimental setup: (A) schematic diagram of the flow system, (B) hot-water tank with temperature control, and (C) helical coil test section with thermocouple locations and data acquisition system.

2.4 Computational Fluid Dynamics Model

Computational fluid dynamics (CFD) was used to extend the analysis from the three experimental coil samples to nine geometrical cases, namely FC-1 to FC-9. These cases were arranged as a design matrix based on tube cross-sectional geometry and coil curvature, as presented in Tables 2 and 3.

Table 2. Geometrical parameters of helical coil samples used for CFD simulations

Sample	δ (%)	D_h/D_{coil}	D_h (m)	D_{coil} (m)	Surface area (m^2)	Length (m)	Elements (cell)
FC-1	66.67	0.062	0.0111	0.1800	0.1121	2.2457	2,161,369
FC-2	66.67	0.065	0.0111	0.1710	0.1068	2.1331	2,056,715
FC-3	66.67	0.067	0.0111	0.1660	0.1038	2.0705	2,007,803
FC-4	33.33	0.062	0.0120	0.1940	0.1173	2.4210	1,625,947
FC-5	33.33	0.065	0.0120	0.1851	0.1121	2.3083	2,131,457
FC-6	33.33	0.067	0.0120	0.1800	0.1093	2.2457	1,542,284
FC-7	50.00	0.062	0.0117	0.1884	0.1154	2.3459	1,859,269
FC-8	50.00	0.065	0.0117	0.1800	0.1107	2.2457	1,784,914
FC-9	50.00	0.067	0.0117	0.1744	0.1072	2.1706	1,725,685

Table 3. Classification of helical coil samples for CFD analysis based on ovality (δ) and geometric ratio (D_h/D_{coil})

δ (%)	D_h/D_{coil} = 0.062	D_h/D_{coil} = 0.065	D_h/D_{coil} = 0.067
66.67	FC-1	FC-2	FC-3
50.00	FC-7	FC-8	FC-9
33.33	FC-4	FC-5	FC-6

The CFD model was developed using ANSYS Fluent within the ANSYS Workbench environment. The finite volume method was applied to solve the governing equations of mass, momentum, and energy conservation. The flow inside the coil was assumed to be steady-state and incompressible, and the thermophysical properties of water were treated as constant at the average system temperature. These assumptions enabled systematic comparison among different geometrical cases. Turbulence was modeled using the Shear Stress Transport (SST) $k-\omega$ model. This model was selected because near-wall prediction is important for the present heat-transfer problem, where wall-adjacent velocity gradients, curvature-induced pressure variations, and secondary-flow development influence the thermal behavior [11, 12]. A recent CFD validation study of turbulent internal tube flow has also demonstrated the applicability of the SST model, together with appropriate near-wall mesh resolution, for heat-transfer prediction [13]. Although the standard $k-\varepsilon$ model is widely used in engineering turbulent-flow simulations and was considered as an alternative, the $SST\ k-\omega$ model was selected for the present curved-coil geometry because of the importance of near-wall flow and curvature-induced flow redistribution. No separate turbulence-model sensitivity study was performed in the present work; therefore, no comparative superiority of the $SST\ k-\omega$ model over other turbulence models is claimed. Instead, the suitability of the selected model was assessed through direct quantitative comparison of the CFD predictions with the experimental data of this study, as described in Section 2.7. The standard model constants were used without additional tuning. The boundary conditions were defined to be consistent with the experimental setup. The inlet flow rate was varied from 0.5 to 2.5 L/min, and the inlet fluid temperature was set to 50 °C, consistent with the experimental condition. The outlet was specified as a pressure outlet, while the tube wall was treated as a no-slip boundary. A constant temperature of 30 °C was imposed on the outer coil surface to represent the controlled thermal condition used in the experiments. Mesh resolution was selected to capture the near-wall flow and curvature-induced secondary-flow behavior adequately. The number of elements used for each geometrical configuration is listed in Table 2. A mesh independence study was performed by increasing the mesh size from approximately 1.37×10^6 to 2.72×10^6 cells and monitoring the resulting Nusselt number. The variation in Nu remained below approximately 1.6% beyond a mesh size of about 1.54×10^6 cells, indicating that further mesh refinement had only a limited effect on the predicted heat-transfer performance. Detailed mesh-independence results are presented in Section 2.7 and Table 6.

2.5 Heat Transfer Calculation and Dimensionless Parameters

The heat transfer performance of the elliptical helical coil was evaluated from the energy change of the working fluid flowing through the coil. The heat transfer rate was calculated from the mass flow rate, specific heat capacity, and temperature difference between the coil inlet and outlet, as expressed in Equation (3).

$$Q = \dot{m}C_p(T_{in} - T_{out}) \tag{3}$$

where $\dot{m}$ is the fluid mass flow rate, C_p is the specific heat capacity of the working fluid, and T_{in} and T_{out} are the fluid temperatures at the coil inlet and outlet, respectively. The bulk mean temperature of the working fluid inside the coil, T_B, was defined as the average of the inlet and outlet temperatures, as given in Equation (4).

$$T_B = \frac{T_{in}+T_{out}}{2} \tag{4}$$

The driving temperature difference for internal convection was defined as the difference between the bulk mean fluid temperature and the average coil surface temperature, as expressed in Equation (5).

$$\Delta T_m = T_B - T_s \tag{5}$$

where T_s is the average coil surface temperature measured using thermocouples installed on the coil surface. The internal heat transfer coefficient, h, was then calculated using Equation (6).

$$h = \frac{Q}{A_i \Delta T_m} \tag{6}$$

where A_i is the internal heat transfer area of the helical coil.

To compare the heat transfer performance of coils with different geometries on a consistent basis, the heat transfer coefficient was expressed in dimensionless form as the Nusselt number. The hydraulic diameter, D_h, was used as the characteristic length, as shown in Equation (7).

$$Nu = \frac{hD_h}{k} \tag{7}$$

where k is the thermal conductivity of the working fluid.

The flow condition inside the coil was characterized using the Reynolds number (Re), which represents the relative strength of inertial to viscous effects in the tube flow, as defined in Equation (8).

$$Re = \frac{\rho u D_h}{\mu} \tag{8}$$

where ρ is the density of the working fluid, u is the mean fluid velocity inside the tube, and μ is the dynamic viscosity of the working fluid.

Because a helical coil is a curved tube, its flow behavior cannot be described by the Reynolds number alone. The coil curvature also contributes to the development of secondary flow. Therefore, the Dean number (Dn) was used to represent the tendency of the flow to generate secondary motion inside elliptical helical coils, as defined in Equation (9).

$$Dn = Re\left(\frac{D_h}{D_{coil}}\right)^{1/2} \tag{9}$$

where D_{coil} is the coil diameter.

The Prandtl number (Pr) was also included to describe the ratio of momentum diffusivity to thermal diffusivity of the working fluid, as defined in Equation (10).

$$Pr = \frac{\mu C_p}{k} \tag{10}$$

The dimensionless parameters Re, Dn, Pr, and Nu were used as the main quantitative indicators for analyzing both the experimental and CFD results. Together, these parameters provide a systematic description of the flow regime, secondary-flow development, and heat transfer performance of the helical coil. They also allow elliptical coils with different geometrical configurations to be compared using a common analytical basis. The pressure loss across the helical coil was also evaluated from the CFD results to examine the hydraulic effect of the investigated geometrical configurations. The pressure loss was determined from the difference between the area-weighted average static pressures at the inlet and outlet:

$$\Delta P = P_{in} - P_{out} \tag{11}$$

where P_{in} and P_{out} are the area-weighted average static pressures at the coil inlet and outlet, respectively. The pressure-loss analysis was used to identify hydraulic trends and was not included in the development of the Nusselt number correlation.

2.6 Model Accuracy Evaluation

The accuracy of the CFD model and the developed correlation was evaluated by comparing the predicted Nu with the corresponding reference values obtained from either CFD results or experimental data, depending on the purpose of each comparison. Four statistical indicators were used: mean absolute percentage error ($MAPE$), root mean square error ($RMSE$), coefficient of determination (R^2), and $adjusted\ R^2$. These metrics were selected to quantify both the prediction error and the ability of the model to represent the overall

data trend. The combined use of statistical error indicators and cross-validation is consistent with model assessment practices reported in previous studies on flow and heat transfer prediction in helical coils [14]. The $MAPE$ was used to quantify the average relative deviation between the predicted and reference values, as calculated using Equation (12).

$$MAPE(\%) = \frac{1}{N}\sum_{i=1}^{N}\left|\frac{Nu_{ref,i}-Nu_{pred,i}}{Nu_{ref,i}}\right| \times 100 \quad (12)$$

The $RMSE$ was used to quantify the overall magnitude of the prediction error relative to the reference values, as defined in Equation (13).

$$RMSE = \sqrt{\frac{1}{N}\sum_{i=1}^{N}\left(Nu_{ref,i} - Nu_{pred,i}\right)^2} \quad (13)$$

The coefficient of determination, R^2, was used to evaluate how well the model explains the variation and overall trend of the reference data, as calculated using Equation (14).

$$R^2 = 1 - \frac{\sum_{i=1}^{N}\left(Nu_{ref,i}-Nu_{pred,i}\right)^2}{\sum_{i=1}^{N}\left(Nu_{ref,i}-\overline{Nu}_{ref}\right)^2} \quad (14)$$

In addition, the adjusted R^2 was used to assess the explanatory performance of the model while accounting for the number of independent variables included in the regression. This metric is particularly useful for models involving multiple predictors and was calculated using Equation (15).

$$Adjusted\ R^2 = 1 - (1 - R^2)\frac{N-1}{N-p-1} \quad (15)$$

where N is the total number of data points, $Nu_{ref,i}$ is the reference Nusselt number for the $i-th$ data point, $Nu_{pred,i}$ is the Nusselt number predicted by the model, $\overline{Nu}_{ref}$ is the mean reference Nusselt number, and p is the number of independent variables included in the model. Cross-validation was also performed to examine the stability of the model when applied to data not directly used in the fitting process.

2.7 Reliability Assessment of Experimental Data, Mesh Independence, and CFD Model Validation

Before using the CFD results for further geometrical analysis, the reliability of the experimental data and the applicability of existing correlations were first examined. These correlations were originally developed for circular helical coils or curved tubes. The experimental Nusselt numbers (Nu_{EXP}) obtained from the three elliptical helical coil samples, namely FC-1EXP, FC-2EXP, and FC-3EXP, were compared with correlations reported in the literature. The selected correlations included those of Xin and Ebadian [15], Schmidt [16], Pawar and Sunnapwar [17], Dravid et al. [18], and Pimenta and Campos [19], as summarized in Table 4. These correlations were not used to directly represent the behavior of elliptical coils. Instead, they served as reference baselines to evaluate how well correlations developed from circular tube geometries can describe the heat transfer behavior of elliptical helical coils.

Table 4. Existing Nusselt number correlations used as reference baselines for elliptical helical coil data

Model	Correlation	Original conditions and range
Xin & Ebadian [15]	$Nu = (2.153 + 0.318Dn^{0.643})Pr^{0.177}$	D/d=11.3–37.5, Dn=20–2000, Pr=0.7–175, peripheral average, constant heat flux
Schmidt [16]	$Nu = 3.65 + 0.08\left[1 + 0.8\left(1 + \frac{d}{D}\right)\left(\frac{d}{D}\right)^{0.9}\right]Re^{\left[0.5+0.2903\left(\frac{d}{D}\right)^{0.1}\right]}Pr^{\frac{1}{3}}$	$100<Re<Re_{cr}$
	$Nu = 0.023\left[1 + 14.8\left(1 + \frac{d}{D}\right)\left(\frac{d}{D}\right)^{\frac{1}{3}}\right]Re^{[0.8-0.22(d/D)^{0.1}]}Pr^{\frac{1}{3}}$	$Re_{cr}<Re<22000$
	$Nu = 0.023\left[1 + 3.6\left(1 - \frac{d}{D}\right)\left(\frac{d}{D}\right)^{0.8}\right]Re^{0.8}Pr^{\frac{1}{3}}$	$20000<Re<150000$
Pawar & Sunnapwar [17]	$Nu = 0.0472Dn^{0.8346}Pr^{0.4}$	Dn=586–4773, Pr=3.83–7.3, constant wall temperature
Dravid et al. [18]	$Nu = (0.76 + 0.65Dn^{0.5})Pr^{0.175}$	D/d=18.67, Dn=50–2000, Pr=5–175, constant heat flux
Pimenta & Campos [19]	$Nu = (0.5Dn^{0.481} - 0.465)Pr^{0.367}$	D/d=40.19, Re=91–6293, Pr=10–353, constant wall temperature

Note: In the Schmidt correlation, Re_{cr} denotes the critical Reynolds number used to distinguish the flow regimes in the helical coil [20]. It was calculated as: $Re_{cr} = 2300[1 + 8.6(d/D)^{0.45}]$ [16]

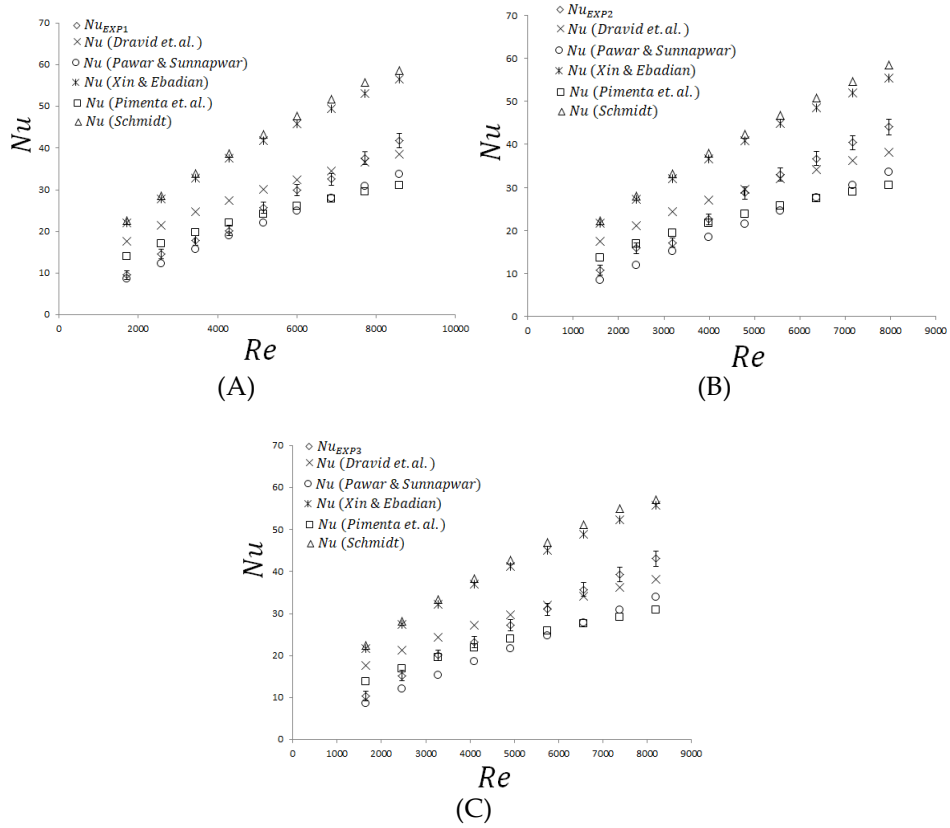


Figure 5. Validation of Nusselt number (Nu) as a function of Reynolds number (Re) for (A) FC-1EXP, (B) FC-2EXP, and (C) FC-3EXP compared with empirical correlations from the literature.

The predicted values from the correlations listed in Table 4 were compared with the experimental Nusselt numbers (Nu_{EXP}) of FC-1EXP, FC-2EXP, and FC-3EXP, as shown in Figure 5A–C. The comparison shows that Nu_{EXP} increases with Re, which is consistent with the basic convective heat transfer behavior in helical coils. However, from a quantitative perspective, several existing correlations produced deviations that were clearly larger than the experimental uncertainty range of ±4–11%. The prediction accuracy of each correlation is summarized in Table 5.

Table 5. Accuracy of existing Nusselt number correlations against elliptical helical coil experimental data

Model	RMSE	MAPE (%)	R^2	Interpretation
Xin & Ebadian [15]	14.2781	62.8588	-0.8072	Not suitable
Schmidt [16]	17.4993	69.7701	-1.7146	Not suitable
Pawar & Sunnapwar [17]	3.5074	13.0986	0.891	Best existing correlation
Dravid et al. [18]	4.8522	23.3517	0.7913	Moderate agreement
Pimenta & Campos [19]	6.4277	18.4098	0.6338	Limited agreement

From Table 5, the correlations of Xin and Ebadian and Schmidt showed the lowest agreement with the experimental data, with $MAPE$ values higher than 60% and negative. R^2 values. This indicates that these two correlations could not adequately represent the trend of the elliptical-coil experimental data. In contrast, the correlation of Pawar and Sunnapwar provided the best performance among the existing correlations, with a $MAPE$ of 13.10% and R^2= 0.891. Nevertheless, this error was still higher than the experimental uncertainty range, confirming that correlations developed for circular helical coils remain limited when directly applied to elliptical helical coils. These results suggest that existing correlations can serve as reference baselines for checking the general trend of Nu, but they are not sufficient for quantitative prediction in elliptical helical coils. Therefore, the experimental data from FC-1EXP, FC-2EXP, and FC-3EXP were used as the main reference for validating the CFD model before extending the analysis to additional geometrical cases. After establishing

the experimental data as the validation reference, the reliability of the numerical results was further assessed through a mesh independence test. The Nu was selected as the main evaluation parameter because it directly reflects the heat transfer performance of the helical coil [21]. In this test, the number of mesh elements was gradually increased from 1.37×10^6 to 2.72×10^6 cells, as shown in Table 6.

Table 6. Grid independence study based on Nusselt number (Nu) for different mesh densities

Number of elements (cells)	1,377,250	1,502,983	1,518,920	1,542,284	2,133,504	2,715,783
Nu_{CFD}	11.54	11.30	11.28	11.17	11.00	11.05
ΔNu_{CFD} from previous mesh (%)	-	2.08	0.18	0.98	1.52	0.45

Note: ΔNu_{CFD} represents the relative change in Nu_{CFD} compared with the preceding mesh density.

The mesh independence results showed that Nu remained within a relatively narrow range as the number of elements increased. Across the tested mesh range, Nu varied from 11.54 to 11.05. The relative change between successive mesh levels was 2.08%, 0.18%, 0.98%, 1.52%, and 0.45%, respectively. Beyond approximately 1.54×10^6 cells, the variation in Nu remained below approximately 1.6%, indicating that further mesh refinement produced only a limited effect on the predicted heat-transfer performance. Therefore, meshes within this range were considered suitable for the main simulations, providing a reasonable balance between numerical accuracy and computational cost. After the mesh independence assessment, the CFD model was quantitatively validated against the experimental Nusselt number data obtained from FC-1EXP, FC-2EXP, and FC-3EXP, which correspond to the geometrically matching CFD cases FC-1, FC-6, and FC-8, respectively. The comparison was conducted at nine corresponding flow-rate conditions ranging from 0.50 to 2.50 L/min, resulting in a total of 27 paired experimental–CFD data points. The agreement was evaluated using $MAPE$, $RMSE$, R^2 and the maximum absolute percentage deviation. The $MAPE$ values for FC-1EXP/FC-1, FC-2EXP/FC-6, and FC-3EXP/FC-8 were 4.75%, 5.03%, and 4.72%, respectively, with corresponding R^2 values of 0.980, 0.980, and 0.982. Considering all 27 validation pairs together, the CFD model yielded an overall $MAPE$ of 4.83%, an $RMSE$ of 1.47, and an R^2 of 0.981, with a maximum absolute deviation of 11.04%. These results indicate reasonable quantitative agreement between the CFD predictions and the experimental measurements and support the use of the validated CFD model for the subsequent analysis of the extended geometrical matrix.

Table 7. Quantitative validation of CFD-predicted Nusselt numbers against experimental data

Experimental	Matching CFD	$MAPE$ (%)	$RMSE$	R^2	Maximum deviation (%)
FC-1EXP	FC-1	4.75	1.46	0.980	8.23
FC-2EXP	FC-6	5.03	1.55	0.980	11.04
FC-3EXP	FC-8	4.72	1.39	0.982	8.88
Overall	27 pairs	4.83	1.47	0.981	11.04

2.8 Development of the Nusselt Number Correlation

The Nu correlation was developed using a dataset of 81 CFD data points obtained from nine geometrical configurations (FC-1 to FC-9), with each configuration evaluated at nine flow-rate conditions ranging from 0.5 to 2.5 L/min. The nine configurations covered three cross-sectional ovality ratios and three values of D_h/D_{coil}, as defined in the design matrix. In addition, 27 experimental data points were obtained from three elliptical coil configurations, with each configuration tested at nine flow-rate conditions ranging from 0.50 to 2.50 L/min. These experimental data were used independently as physical reference data for validating the CFD model. The 81 CFD data points used for correlation development were expressed in terms of dimensionless parameters, allowing coils with different geometries to be compared on a consistent basis. The independent variables used in the correlation included the Dn, Pr, δ, and the coil geometric ratio (D_h/D_{coil}). These variables represent the combined effects of flow behavior, fluid properties, and coil geometry. The correlation was formulated as a power-law model, as expressed in Equation (16) [22, 23].

$$Nu = CDn^a \left(\frac{Pr}{Pr_{ref}}\right)^b \delta^c \left(\frac{D_h}{D_{coil}}\right)^d \quad (16)$$

where C is the model constant, and a, b, c, and d are the exponents to be estimated from the dataset. The term Pr_{ref} is the reference Prandtl number used to normalize Pr, helping reduce the effect of its narrow data range and improving the stability of the regression. The parameter δ was expressed in decimal form, where 33.33%, 50.00%, and 66.67% correspond to 0.3333, 0.5000, and 0.6667, respectively, to ensure consistency in the regression calculation. To estimate the model parameters, Equation (16) was transformed into a linear form by taking the natural logarithm of both sides, as shown in Equation (17) [22, 24].

$$\ln Nu = \ln C + a \ln Dn + b \ln\left(\frac{Pr}{Pr_{ref}}\right) + c \ln \delta + d \ln\left(\frac{D_h}{D_{coil}}\right) \quad (17)$$

Multiple linear regression was then applied together with least-squares fitting to estimate the model constant and exponents. The accuracy of the developed correlation was evaluated using statistical indicators, including R^2, $adjusted\ R^2$, $RMSE$, $MAPE$, and cross-validation. These metrics were used to assess both the ability of the model to describe the data trend and the quantitative error of the predicted values.

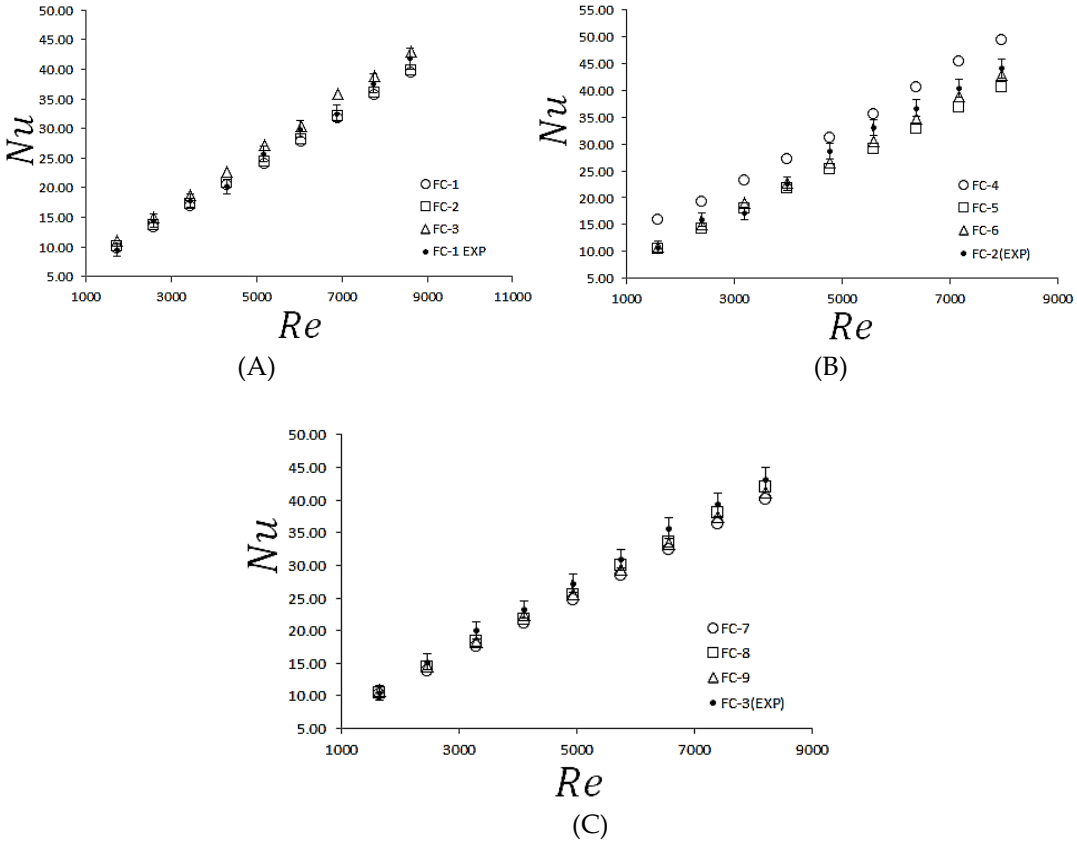


Figure 6. Variation of Nusselt number (Nu) with Reynolds number (Re) for different ovality ratios: (A) δ = 66.67%, (B) δ = 33.33%, and (C) δ = 50.00%, with experimental data included for comparison.

3. Results and Discussion

3.1 Effect of Reynolds Number on Nusselt Number

Following the quantitative validation of the CFD model against the experimental data, the results from cases FC-1 to FC-9 were used to examine the relationship between Re and Nu under different ovality ratios, as shown in Figure 6. The experimental data included in the same figure were used as a reference to confirm that the $Nu - Re$ trend predicted by CFD is consistent with the behavior observed in the physical system. Figure 6 shows that Nu increases with Re for all investigated configurations, consistent with previous observations that increasing flow intensity enhances convective heat transfer in helical coils through stronger mixing and thermal boundary-layer disruption [25, 26]. However, the differences among the present configurations become more pronounced as Re increases, indicating that the heat-transfer response is not governed by flow

intensity alone. Variations in δ and D_h/D_{coil} modify how curvature-induced secondary flow redistributes momentum within the tube cross-section and interacts with the thermal boundary layer. Consequently, configurations operated at comparable flow intensities can exhibit different Nu values because their geometries produce different internal flow structures. This flow–geometry interaction provides the physical basis for including both flow-related and geometrical parameters in the correlation developed in this study.

3.2 Velocity Field Distribution and Secondary Flow Behavior

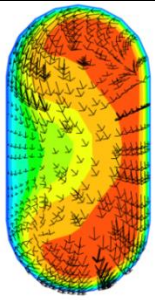
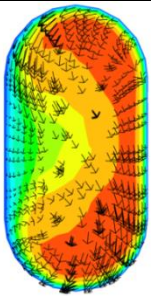
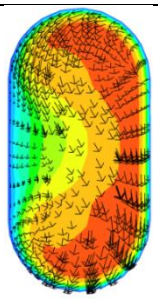
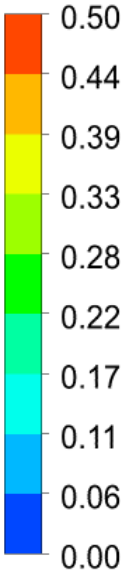
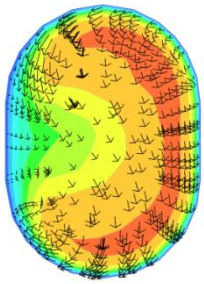
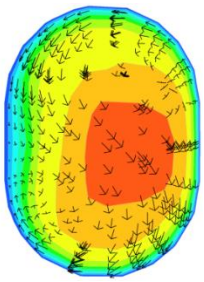
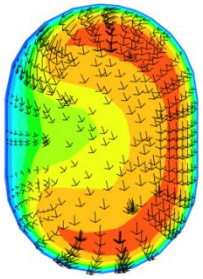
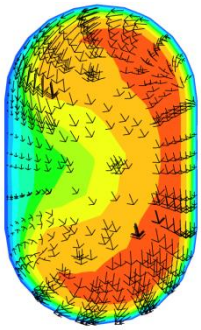
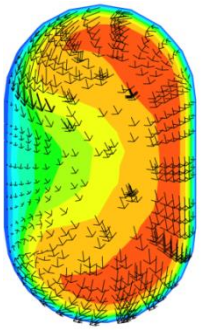
To clarify the mechanism responsible for the differences in heat transfer performance, the velocity field within each helical coil cross-section was analyzed using the CFD results at a flow rate of 2.5 L/min, as presented in Table 8. The comparison of FC-1 to FC-9 shows that coil geometry affects not only the heat transfer magnitude, but also the internal flow structure within the tube cross-section. The velocity field was asymmetric in all cases, with the high-velocity region shifting toward the outer wall of the curved tube. This behavior confirms the effect of centrifugal force and the formation of curvature-induced secondary flow, commonly known as Dean vortices. These vortices enhance fluid mixing and disturb the thermal boundary layer near the tube wall, thereby improving convective heat transfer. The results in Table 8 show that both δ and D_h/D_{coil} influence the intensity and distribution of the velocity field. In the high-ovality group (δ=66.67%), represented by FC-1 to FC-3, the velocity field showed stronger asymmetry and more concentrated high-velocity regions. In the low-ovality group (δ=33.33%), represented by FC-4 to FC-6, the velocity distribution was broader across the cross-section, although asymmetry remained because of coil curvature. The intermediate-ovality group (δ=50.00%), represented by FC-7 to FC-9, showed a transitional pattern between these two behaviors. These observations indicate that changing the tube cross-section alters not only the intensity of secondary motion but also the location and distribution of the high-velocity region within the cross-section. This redistribution is important because it changes the interaction between the core flow and the wall-adjacent region, thereby influencing thermal boundary-layer disturbance and the resulting heat-transfer response. The velocity-field results therefore provide a mechanistic explanation for the geometry-dependent differences in Nu observed in Figure 6.

3.3 Effect of Geometrical Ratio on the Relationship Between Dean Number and Heat Transfer Coefficient

After examining secondary-flow behavior through the velocity field distribution, the Dn was used as a quantitative parameter to evaluate the combined effect of flow intensity and coil curvature on heat transfer performance. The relationship between Dn and h was analyzed under different values of D_h/D_{coil}, as shown in Figure 7.

Figure 7 shows that h increases with Dn for all three. D_h/D_{coil} groups, indicating a strong contribution of curvature-induced flow to convective heat transfer. Nevertheless, the magnitude and slope of the $Dn - h$ relationship differ among the geometrical configurations. Thus, similar values of Dn do not necessarily produce identical h values, showing that geometrical characteristics modify the heat-transfer response beyond the effect represented by Dn alone. This behavior is consistent with the velocity-field results in Section 3.2 and the geometry-dependent $Nu - Re$ behavior discussed in Section 3.1. These findings support the inclusion of Dn, δ, and D_h/D_{coil} as complementary parameters in the subsequent Nu correlation.

Table 8. Comparison of velocity field distributions in helical coil cross-sections at a flow rate of 2.5 L/min for different ovality ratios (δ) and geometric ratios (D_h/D_{coil}).

δ (%)	D_h/D_{coil} = 0.062	D_h/D_{coil} = 0.065	D_h/D_{coil} = 0.067	Scale (m/s)
66.67	 FC-1	 FC-2	 FC-3	 0.50 0.44 0.39 0.33 0.28 0.22 0.17 0.11 0.06 0.00
33.33	 FC-4	 FC-5	 FC-6	
50.00	 FC-7	 FC-8	 FC-9	

3.4 Development and Evaluation of the Nusselt Number Correlation

Based on the coupled flow–geometry effects identified in Sections 3.1–3.3, a Nu correlation was developed to incorporate flow condition, fluid properties, and coil geometry within a single predictive model. Following the regression procedure described in Section 2.8, the developed correlation is expressed as Equation (18).

$$Nu = 0.00843Dn^{0.9754}\left(\frac{Pr}{4.1792}\right)^{9.4961}\delta^{-0.2242}\left(\frac{D_h}{D_{coil}}\right)^{-0.3452} \quad (18)$$

The developed correlation showed high predictive accuracy, with R^2=0.972, $MAPE$=5.36%, and $RMSE$ = 1.84 when evaluated against the dataset used for model development. Cross-validation further produced R^2=0.956 and $MAPE$ = 5.94%, indicating that the correlation can predict data not directly included in each fitting step. These results confirm the stability of the model and show that its performance was not limited only to the dataset used to derive the correlation.

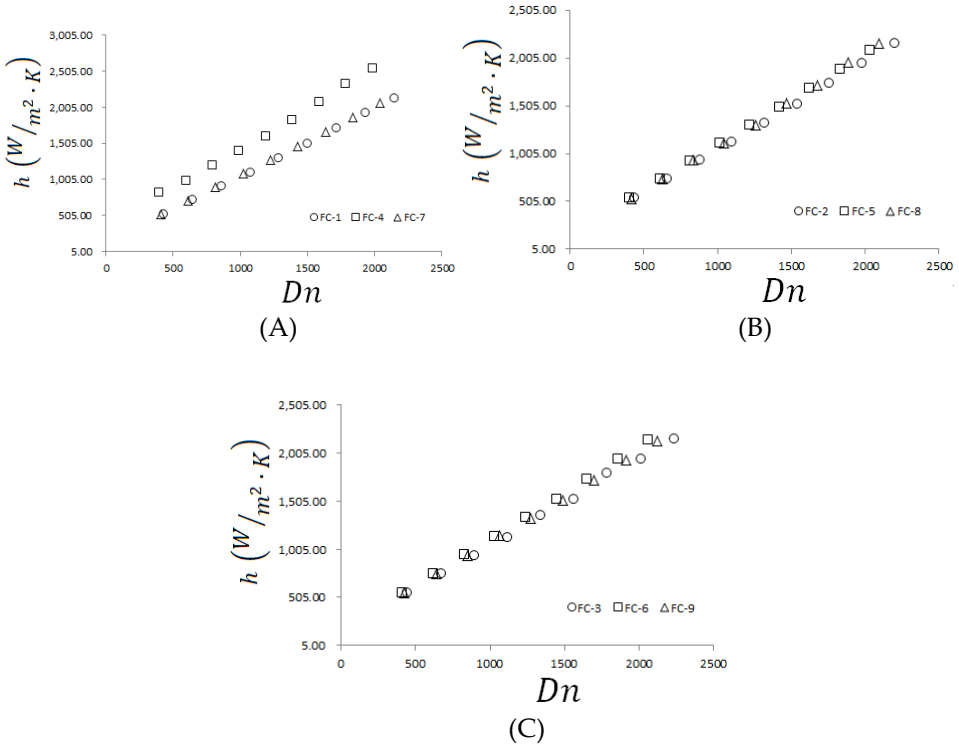


Figure 7. Effect of geometric ratio (D_h/D_{coil}) on the relationship between Dean number (Dn) and heat transfer coefficient (h) obtained from CFD simulations: (A) $D_h/D_{coil} = 0.062$, (B) $D_h/D_{coil} = 0.065$, and (C) $D_h/D_{coil} = 0.067$.

Table 9. Accuracy comparison of the proposed Nu correlation with published correlations and predictive models

Model/study	System/model type	Main accuracy indicator	Interpretation
Present model	Elliptical helical coil, regression correlation	R^2=0.972, $RMSE$=1.84 $MAPE$=5.36%	High agreement
Present model, cross-validation	Same model	R^2=0.956 MAPE=5.94%	Stable prediction
Zakeralhoseini et al. [27]	Helically coiled tube correlation	95% data within ±15% AAD = 5.0	Comparable engineering accuracy
Yadav et al., MLP-NN [28]	Spirally coiled tube, AI model	$MAPE$=4.60%	Similar accuracy level
Yadav et al., ANFIS [28]	Spirally coiled tube, AI model	$MAPE$=6.80%	Similar accuracy level
Existing correlations in Yadav et al. [28]	Published correlations	$MAPE$=25.86–38.51%	Limited transferability

Compared with published studies, the accuracy of the present model falls within an acceptable range for engineering applications. Its prediction error is comparable to those reported for correlations and predictive models developed for helical or spiral coiled tubes in the literature. At the same time, the results in Table 9 indicate that existing correlations may produce considerably larger errors when the geometry or flow conditions differ from the database on which they were originally developed. Therefore, incorporating the geometrical parameters of elliptical helical coils together with flow-related variables is physically reasonable

and improves the prediction of Nu within the investigated parameter range. Beyond the statistical accuracy summarized in Table 9, the structure of Equation (18) also provides physical insight into the role of each variable in determining Nu. In particular, the sign and magnitude of the exponents reflect the combined influence of flow mechanisms and coil geometry. The positive exponent of Dn, which is close to unity (0.9754), indicates that the flow and curvature effects represented by Dn have a strong influence on the predicted Nu within the investigated range. By contrast, the negative exponents of δ and D_h/D_{coil} indicate inverse relationships with the predicted Nu within the investigated parameter range. These effects should be interpreted as geometry-dependent modifications of the heat-transfer response rather than as evidence that either geometrical parameter independently suppresses heat transfer. The Pr term should be interpreted mainly as a scaling factor rather than a primary controlling variable, because the Pr range in the present dataset is relatively narrow. The consistency of the model is further shown in Figure 8. The Nu values predicted by the proposed correlation follow the CFD and experimental data more closely than the existing correlations, particularly in the high-Dn range. In addition, Figure 9 presents the parity plot between Nu_{pred} and Nu_{CFD}, where most data points lie close to the $y = x$ line and within the ±15% error band. These results support that the proposed model provides a suitable level of accuracy for engineering use within the range of parameters investigated in this study.

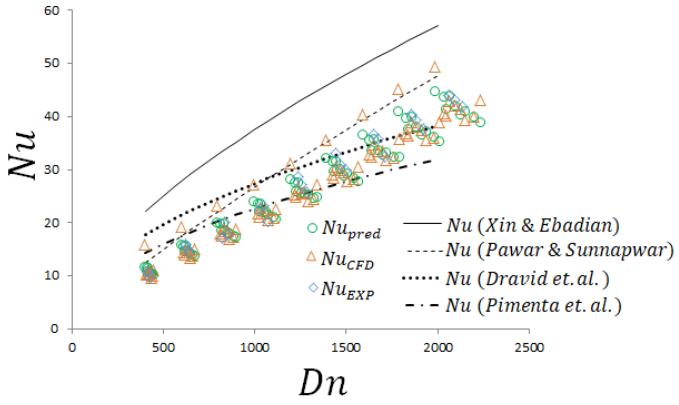


Figure 8. Comparison of Nusselt number (Nu) predicted by the developed correlation with CFD and experimental data.

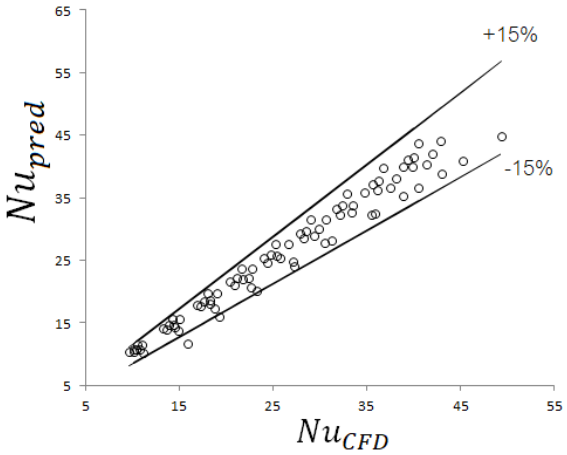


Figure 9. Parity plot comparing the Nusselt number predicted by the developed correlation with CFD data, including the ±15% error band.

3.5 Pressure Loss Characteristics

Figure 10 shows the relationship between pressure loss (ΔP) and Reynolds number (Re) for the nine elliptical helical coil configurations. The pressure loss increased continuously with increasing Re for all configurations. At the lowest investigated flow condition, ΔP was approximately 73–86 Pa, whereas at the

highest flow condition it increased to approximately 749–869 Pa. This nonlinear increase indicates that hydraulic resistance becomes increasingly significant as the flow intensity increases. Differences in pressure loss were also observed among the coil geometries. At the highest investigated flow condition, FC-1 exhibited the largest pressure loss, approximately 869 Pa, whereas FC-9 showed the lowest value, approximately 749 Pa. However, the variation in ΔP with D_h/D_{coil} was not strictly monotonic for all ovality groups. This indicates that hydraulic resistance is controlled by the combined effects of cross-sectional shape, coil curvature, and the resulting flow redistribution rather than by a single geometrical parameter. These results complement the heat-transfer and velocity-field analyses by showing that geometrical modifications affecting secondary-flow behavior also influence the hydraulic resistance of the coil. Therefore, heat-transfer enhancement should be considered together with the associated pressure-loss penalty when elliptical helical coils are applied in practical systems. A complete thermo-hydraulic optimization, however, is beyond the scope of the present study.

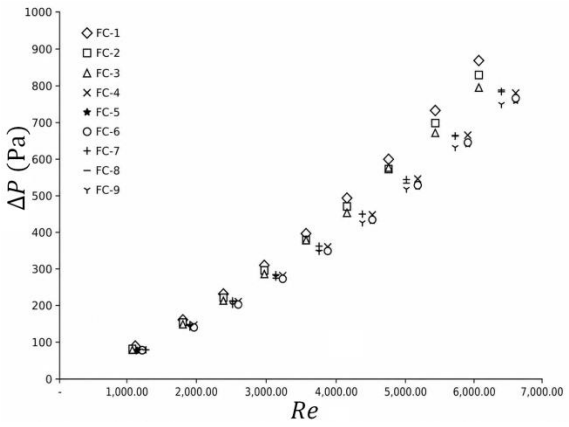


Figure 10. Pressure loss (ΔP) as a function of Reynolds number (Re) for the nine elliptical helical coil configurations.

3.6 Sensitivity Analysis of Variables Affecting the Nusselt Number

A sensitivity analysis was performed to clarify the relative influence of each variable in the developed correlation. Each variable was varied within the actual range obtained from the CFD dataset, while the remaining variables were fixed at the reference condition (Dn = 1124.92, Pr = 4.1792, δ = 0.5000, and D_h/D_{coil} = 0.065), as shown in Figure 11A-D. Among all variables, Dn had the strongest influence on the predicted Nusselt number. (Nu_{pred}). Increasing Dn produced a clear increase in Nu_{pred}, indicating the strong influence of flow intensity and curvature-related effects on the predicted heat-transfer response. The effects of δ and D_h/D_{coil} were more geometry-dependent. Increasing δ produced a gradual decrease in Nu_{pred} over the investigated range, whereas the influence of D_h/D_{coil} was comparatively smaller. This indicates that Dn captures the principal flow–curvature effect, while δ and D_h/D_{coil} provide additional geometrical modulation of the predicted heat-transfer response. The effect of Pr should be interpreted with caution because its range in the present dataset was narrow. Therefore, Pr mainly acts as a fluid-property scaling term rather than a primary variable controlling the flow structure.

3.7 Limitations and Scope of Application

Although the correlation developed in this study can accurately predict the Nu of elliptical helical coils within the investigated dataset, its application should remain within the range of parameters used for model development. The model was derived from experimental data obtained from three elliptical coil configurations and CFD data obtained from nine geometric cases, covering the specified ranges of Dn, Pr, δ, and D_h/D_{coil}. Therefore, applying this correlation to coils with different geometries, flow ranges, or working fluids should be done with caution. Although pressure loss was additionally examined to identify the hydraulic consequences of the investigated coil geometries, the present study primarily focuses on predicting heat transfer behavior in elliptical helical coils. The pressure-loss results were used only to clarify the hydraulic trends associated with flow rate and coil geometry and were not used to develop a friction-factor correlation or to perform a complete thermo-hydraulic optimization. The present study also does not fully represent the overall performance of the WHHE system, including thermal resistance through the tank wall, non-uniform

coil–tank contact, heat loss to the surroundings, fluid behavior inside the heat-receiving tank, fouling effects, long-term changes in thermal contact quality, or transient operating conditions. For these reasons, the proposed correlation should be used as a preliminary evaluation and design tool for elliptical helical coils within the investigated parameter range, rather than as a universal correlation for all coil types. Any extension to practical systems with different geometries or operating conditions should be supported by additional case-specific experimental or CFD validation.

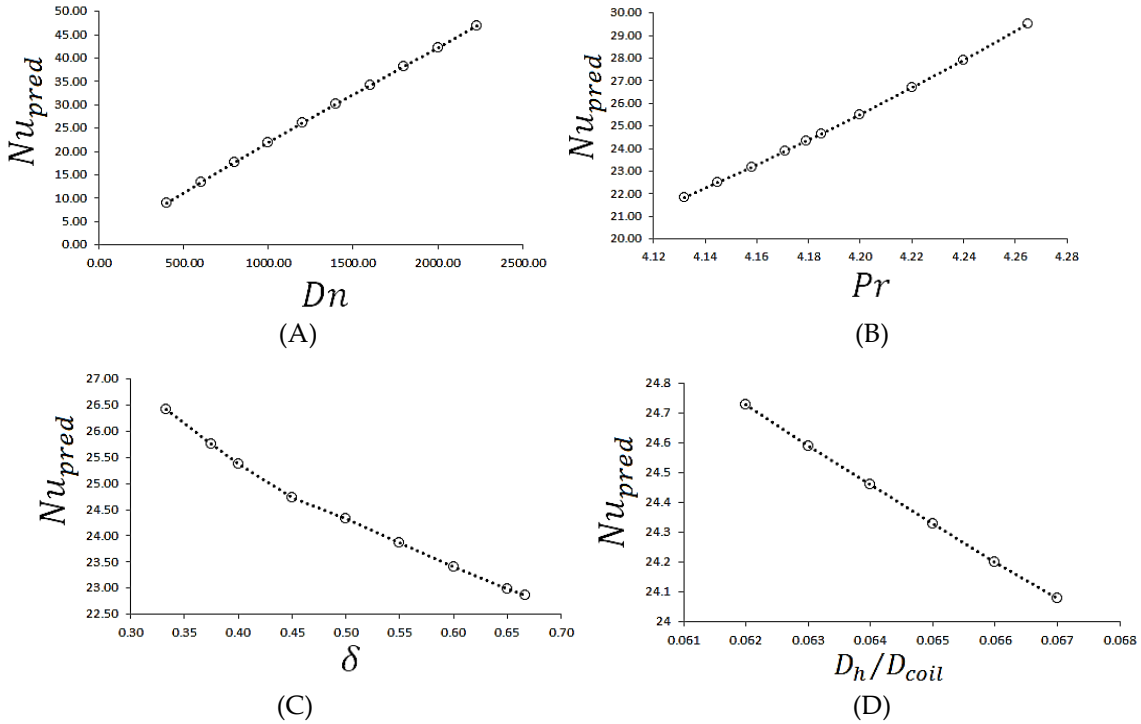


Figure 11. Sensitivity analysis of the predicted Nusselt number (Nu_{pred}) with respect to key parameters: (A) Dean number (Dn), (B) Prandtl number (Pr), (C) ovality (δ), and (D) geometric ratio (D_h/D_{coil}).

4. Conclusions

This study investigated the influence of elliptical helical coil geometry on internal flow behavior and heat-transfer performance using experimental data and CFD simulations. The results showed that Nu increased with Re and Dn, while the velocity-field analysis demonstrated that variations in δ and D_h/D_{coil} modified the internal flow structure and the resulting heat-transfer response. The pressure-loss analysis further showed that hydraulic resistance increased markedly with increasing Reynolds number and varied among the investigated coil geometries, indicating that heat-transfer enhancement should be considered together with the associated pressure-loss penalty. Comparisons with existing circular-coil correlations showed limited quantitative accuracy when directly applied to elliptical helical coils. This confirms the need for a correlation that accounts for the combined effects of flow behavior, cross-sectional shape, and coil curvature. The developed correlation, incorporating Dn, Pr, δ, and D_h/D_{coil}, provided reliable prediction accuracy within the investigated range, with R^2 = 0.972, $MAPE$ = 5.36%, $RMSE$ = 1.84, and a cross-validation $MAPE$ of 5.94%. Overall, the findings show that elliptical helical coils exhibit flow and heat transfer characteristics different from those of circular coils. Therefore, a flow–geometry-coupled correlation provides a suitable basis for predicting Nusselt number and guiding the preliminary design of elliptical helical coils for $WHHEs$ applications within the studied parameter range.

5. Acknowledgments

The authors gratefully acknowledge the institutional support provided by the Department of Mechanical Engineering, Faculty of Engineering, Rajamangala University of Technology Thanyaburi, during the conduct of this study.

Author Contributions: Conceptualization, S.S. and S.T.; methodology, S.S., M.J. and S.T.; data curation, S.S. and S.T.; writing—original draft preparation, S.S.; writing—review and editing, M.J. and S.T.; supervision, M.J. and S.T.; funding acquisition, M.J. and S.T. All authors have read and agreed to the published version of the manuscript.

Funding: This research received no external funding.

Conflicts of Interest: The authors declare no conflict of interest.

References

[1] Flayyih, R. A.; Alwan, K. J.; Aljaberi, H. A. Comparative heat transfer analysis of helical coil and straight tube heat exchangers. *Case Stud. Therm. Eng.* **2025**, *76*, 107386. https://doi.org/10.1016/j.csite.2025.107386

[2] Ying Chua, M. A. Y.; Kumar, P.; Shah, M.; Kurnia, J. C.; Wee, S. K. Heat transfer performance analysis of a helical coil tube with supercritical CO2 as a working fluid. *J. Supercrit. Fluids* **2026**, *228*, 106800. https://doi.org/10.1016/j.supflu.2025.106800

[3] Ghazanfari, V.; Shadman, M. M.; Mansourzade, F.; Amini, Y. Numerical investigation of thermal-hydraulic performance enhancement in helical coil heat exchangers with twisted tube geometries. *Case Stud. Therm. Eng.* **2024**, *60*, 104744. https://doi.org/10.1016/j.csite.2024.104744

[4] Liaw, K. L.; Kurnia, J. C.; Putra, Z. A.; Aziz, M.; Sasmito, A. P. Enhanced turbulent convective heat transfer in helical twisted multilobe tubes. *Int. J. Heat Mass Transfer* **2023**, *202*, 123687. https://doi.org/10.1016/j.ijheatmasstransfer.2022.123687

[5] Gomaa, A.; Gamal, Y.; Abdelmagied, M. M. Enhancement of thermofluid characteristics via a triple-helical tube heat exchanger. *Sci. Rep.* **2025**, *15*(1), 6978. https://doi.org/10.1038/s41598-025-89730-6

[6] Jasim, D. J.; Mahdi, M. S.; Mahdy, O. S.; Basem, A.; Karouei, S. H. H.; Alinia-Kolaei, M. Hydrothermal analysis of hybrid nanofluid flow inside a shell and double coil heat exchanger: Numerical examination. *Int. J. Thermofluids* **2024**, *23*, 100770. https://doi.org/10.1016/j.ijft.2024.100770

[7] Al-Saaidi, H. A. I.; Prieto, C. Influence of helical coil geometry and carbon nanotube additives on the thermal performance of shell-and-helical coiled tube latent heat storage systems. *J. Energy Storage* **2026**, *154*, 121130. https://doi.org/10.1016/j.est.2026.121130

[8] Rahman, M. A. Review on heat transfer augmentation in helically coiled tube heat exchanger. *Int. J. Thermofluids* **2024**, *24*, 100937. https://doi.org/10.1016/j.ijft.2024.100937

[9] Tran, P.-L.; Seong, M.-H.; Kang, S.-C.; Kim, J.-K. Analysis of collapse response of offshore pipes under external pressure and bending considering sizing effect. *Ocean Eng.* **2026**, *351*, 124368. https://doi.org/10.1016/j.oceaneng.2026.124368

[10] Chater, H.; Asbik, M.; Mouaky, A.; Koukouch, A.; Belandria, V.; Sarh, B. Experimental and CFD investigation of a helical coil heat exchanger coupled with a parabolic trough solar collector for heating a batch reactor: An exergy approach. *Renewable Energy* **2023**, *202*, 1507–1519. https://doi.org/10.1016/j.renene.2022.11.108

[11] Lai, Y.; Wang, S.; Guo, Y. Numerical study of tube bundle rotational direction effect on flow and heat transfer in helical coil once-through steam generator. *Int. Commun. Heat Mass Transfer* **2024**, *159*, 108277. https://doi.org/10.1016/j.icheatmasstransfer.2024.108277

[12] Xijun, Z.; Kaiwen, Q.; Xiaobin, T. Simulation of flow field characteristics around longitudinally staggered variable-curvature helical coil bundles. *Nucl. Eng. Des.* **2026**, *446*, 114632. https://doi.org/10.1016/j.nucengdes.2025.114632

[13] Kiss, A.; Kiss, B. Validation of CFD models of horizontal and vertical upward water flow in straight tubes under supercritical conditions. *Nucl. Eng. Des.* **2026**, *448*, 114674. https://doi.org/10.1016/j.nucengdes.2025.114674

[14] Cai, L.; Liu, J.; Mi, S.; Xu, C. Interpretable machine learning-based prediction and analysis on flow and heat transfer characteristics of phase change material slurry in helically coiled tube with twisted tape insert for energy storage. *J. Energy Storage* **2025**, *133*, 118016. https://doi.org/10.1016/j.est.2025.118016

[15] Xin, R.; Ebadian, M. The effects of Prandtl numbers on local and average convective heat transfer characteristics in helical pipes. *J. Heat Transfer* **1997**, *119*(3), 467–473. https://doi.org/10.1115/1.2824120

[16] Schmidt, E. F. Wärmeübergang und Druckverlust in Rohrschlangen. *Chem. Ing. Tech.* **1967**, *39*(13), 781–789. https://doi.org/10.1002/cite.330391302

[17] Pawar, S. S.; Sunnapwar, V. K. Experimental studies on heat transfer to Newtonian and non-Newtonian fluids in helical coils with laminar and turbulent flow. *Exp. Therm. Fluid Sci.* **2013**, *44*, 792–804. https://doi.org/10.1016/j.expthermflusci.2012.09.024

[18] Dravid, A. N.; Smith, K.; Merrill, E.; Brian, P. Effect of secondary fluid motion on laminar flow heat transfer in helically coiled tubes. *AIChE J.* **1971**, *17*(5), 1114–1122. https://doi.org/10.1002/aic.690170517

[19] Pimenta, T. A.; Campos, J. B. L. M. Heat transfer coefficients from Newtonian and non-Newtonian fluids flowing in laminar regime in a helical coil. *Int. J. Heat Mass Transfer* **2013**, *58*(1–2), 676–690. https://doi.org/10.1016/j.ijheatmasstransfer.2012.10.078

[20] Chua, M. A. Y. Y.; Kumar, P.; Shah, M. T.; Kurnia, J. C.; Wee, S. K. Computational study of helical coil heat exchanger: Energy, entropy, exergy, entransy (4E) analysis and application of field synergy principle. *Int. J. Refrig.* **2025**, *172*, 41–63. https://doi.org/10.1016/j.ijrefrig.2025.01.026

[21] Ali, S. A.; Jamil Alrikaby, N.; Kadhim, H. K. Computational analysis of dimples surface tube on heat transfer forced convection using turbulence model of low Reynolds number with different cases. *ASEAN J. Sci. Technol. Rep.* **2025**, *28*(3). https://doi.org/10.55164/ajstr.v28i3.256103

[22] Hedau, A.; Singal, S. K. Development of Nusselt number and friction factor correlations for double-pass solar air heater duct. *Appl. Therm. Eng.* **2023**, *234*, 121227. https://doi.org/10.1016/j.applthermaleng.2023.121227

[23] Guo, H.; Zhang, X.; Feng, L.; Wu, Y.; Wu, Y. Experimental Nusselt number correlations for heat transfer of a single spherical particle in turbulent flow. *Int. J. Heat Mass Transfer* **2026**, *256*, 127939. https://doi.org/10.1016/j.ijheatmasstransfer.2025.127939

[24] Shrivastava, A.; Kumar, V. Statistical correlations for Nusselt number and friction factor in rectangular pyramid-shaped roughened solar air collectors. *Int. Commun. Heat Mass Transfer* **2026**, *170*, 109995. https://doi.org/10.1016/j.icheatmasstransfer.2025.109995

[25] Sharipova, A.; Shafiee, M.; Lotfi, M.; Bekturganova, N. Y. Enhanced thermohydraulic performance in helical coil heat exchangers using synthesized Cu-doped TiO2 nanofluids: An experimental approach. *Int. J. Therm. Sci.* **2026**, *220*, 110338. https://doi.org/10.1016/j.ijthermalsci.2025.110338

[26] Abdelmagied, M. Thermo-hydraulic and exergy characteristics of a triple tube helical coil with inner triangular twisted tube. *Int. J. Air-Cond. Refrig.* **2024**, *32*(1). https://doi.org/10.1007/s44189-024-00065-9

[27] Zakeralhoseini, S.; Sajadi, B.; Akhavan Behabadi, M. A.; Azarhazin, S.; Fazelnia, H. Experimental investigation of the heat transfer coefficient and pressure drop of R1234yf during flow condensation in helically coiled tubes. *Int. J. Therm. Sci.* **2020**, *157*, 106516. https://doi.org/10.1016/j.ijthermalsci.2020.106516

[28] Yadav, A.; Doshi, H.; Jayaprakash, B.; Hasan, N. A.; Mohammad, H.; Kundlas, M.; Bharathi, B.; Sahu, P. K.; Vats, S.; Ranjbar, F. Prediction of the heat transfer coefficient during condensation within spirally coiled tubes of various orientations: Artificial intelligence modeling and correlation development. *Int. J. Heat Fluid Flow* **2026**, *119*, 110314. https://doi.org/10.1016/j.ijheatfluidflow.2026.110314